Biochemical and Biophysical Research Communications 464 (2015) 737–742

Contents lists available at ScienceDirect

Biochemical and Biophysical Research Communications

journal homepage: www.elsevier.com/locate/ybbrc

Fluorescence labeled microbubbles for multimodal imaging

Åsa Barrefelt [a, b, 1], Ying Zhao [a, 1], Malin K. Larsson [c], Gabriella Egri [d], Raoul V. Kuiper [e], Jörg Hamm [f], Maryam Saghafian [b], Kenneth Caidahl [g], Torkel B. Brismar [a], Peter Aspelin [a], Rainer Heuchel [a], Mamoun Muhammed [h], Lars Dähne [d], Moustapha Hassan [b, i, *]

[a] Department of Clinical Science, Intervention and Technology (CLINTEC), Karolinska Institutet (KI), Stockholm, Sweden
[b] Experimental Cancer Medicine (ECM), Department of Laboratory Medicine, KI, Sweden
[c] Department of Medical Engineering, School of Technology and Health, Royal Institute of Technology (KTH), Stockholm, Sweden
[d] Surflay Nanotec GmbH, 12489 Berlin, Germany
[e] Karolinska Institute Core Facility for Morphologic Phenotype Analysis, Karolinska University Hospital-Huddinge, Stockholm, Sweden
[f] PerkinElmer, 68 Elm St., Hopkinton, MA 01748, USA
[g] Department of Molecular Medicine and Surgery, KI, Dept. Clin Phys, Karolinska University Hospital, Stockholm, Sweden
[h] Department of Materials and Nano Physics, Division of Functional Materials (FNM), Royal Institute of Technology (KTH), Stockholm, Sweden
[i] Clinical Research Center (KFC, Novum), Karolinska University Hospital-Huddinge, Stockholm, Sweden

ARTICLE INFO

Article history:
Received 23 June 2015
Accepted 2 July 2015
Available online 15 July 2015

Keywords:
In vivo imaging systems
Micro-computed tomography
Micro-ultrasound
Microbubbles
VivoTag 680
Near infrared (NIR)
Fluorescence

ABSTRACT

Air-filled polyvinyl alcohol microbubbles (PVA-MBs) were recently introduced as a contrast agent for ultrasound imaging. In the present study, we explore the possibility of extending their application in multimodal imaging by labeling them with a near infrared (NIR) fluorophore, VivoTag-680.

PVA-MBs were injected intravenously into FVB/N female mice and their dynamic biodistribution over 24 h was determined by 3D-fluorescence imaging co-registered with 3D-μCT imaging, to verify the anatomic location. To further confirm the biodistribution results from *in vivo* imaging, organs were removed and examined histologically using bright field and fluorescence microscopy. Fluorescence imaging detected PVA-MB accumulation in the lungs within the first 30 min post-injection. Redistribution to a low extent was observed in liver and kidneys at 4 h, and to a high extent mainly in the liver and spleen at 24 h. Histology confirmed PVA-MB localization in lung capillaries and macrophages. In the liver, they were associated with Kupffer cells; in the spleen, they were located mostly within the marginal-zone. Occasional MBs were observed in the kidney glomeruli and interstitium.

The potential application of PVA-MBs as a contrast agent was also studied using ultrasound (US) imaging in subcutaneous and orthotopic pancreatic cancer mouse models, to visualize blood flow within the tumor mass.

In conclusion, this study showed that PVA-MBs are useful as a contrast agent for multimodal imaging.

1. Introduction

Nano- and microparticles are on the verge of becoming standard in future medicine. Due to their potential ligation to enhancing agents, such as fluorescent dyes, gold, iron oxide or manganese, and/or antibodies, they have been used as contrast agents and targeted drug delivery vehicles [1–5]. The combination of *in vivo* imaging modalities such as optical *in vivo* imaging/magnetic resonance imaging (MRI) and optical *in vivo* imaging/computed tomography (CT) opens up a new era of non-radioactive agents for functional imaging using a multimodal approach [6]. Adding fluorescent markers to injectable contrast agents carrying a combination of superparamagnetic iron oxide nanoparticles (SPION) for detection by MRI or gold nanoparticles for detection by CT enables their multimodal use [7]. Recently, polyvinyl alcohol microbubbles (PVA-MBs) were introduced as a contrast agent for multimodality or hybrid imaging by combining MRI [6,8], single photon emission computed tomography (SPECT) [8] and ultrasound [9–12].

* Corresponding author. ECM, KFC, Novum, Karolinska University Hospital-Huddinge, SE-141 86 Stockholm, Sweden.
E-mail addresses: asa.barrefelt@ki.se (Å. Barrefelt), ying.zhao.1@ki.se (Y. Zhao), malinl@sth.kth.se (M.K. Larsson), g.egri@surflay.com (G. Egri), Raoul.Kuiper@ki.se (R.V. Kuiper), Jorg.Hamm@perkinelmer.com (J. Hamm), maryam.saghafian@ki.se (M. Saghafian), Kenneth.Caidahl@ki.se (K. Caidahl), torkel.brismar@karolinska.se (T.B. Brismar), Peter.Aspelin@ki.se (P. Aspelin), rainer.heuchel@ki.se (R. Heuchel), mamoun@kth.se (M. Muhammed), l.daehne@surflay.com (L. Dähne), Moustapha.hassan@ki.se (M. Hassan).
[1] Equal contribution from authors.

http://dx.doi.org/10.1016/j.bbrc.2015.07.017
0006-291X/

Functionalized MBs are also suitable for labeling with fluorescent probes, which facilitates pre-clinical biodistribution and kinetic studies in small animals without the need for radio isotopes [13]. The employment of optical *in vivo* imaging based on non-invasive detection of fluorescence or luminescence enables sequential analysis of the same animals, providing dynamic data [14,15] and minimizing inter-individual variation. Optical *in vivo* imaging can complement other imaging modalities such as MRI, ultrasound and CT for multimodal approaches. Fluorescence-based *in vivo* examination of microbubbles can ultimately be verified by fluorescence microscopy [16]. Ling et al. [17] studied streptavidin-based nanoparticles conjugated with up to four biotinylated probes of varying detectional/functional modalities. The authors were able to use a unique combination of simultaneous nuclear medicine and fluorescent imaging in a tissue-targeted approach. Vasquez et al. dynamically imaged and quantified fluorescence-labeled particles in mice using tomographic imaging [15].

The fluorescence quantum yield and high photostability of VivoTag 680 allows detection of low-abundance biological structures in deep tissues with good sensitivity. VivoTag 680 dye molecules can be attached to proteins/nanoparticles and microvehicles at high molar ratios without significant self-quenching, resulting in brighter conjugates and sensitive detection [15]. The long wavelength emission allows for detection in complex samples with little interference from photon absorption by hemoglobin (absorption peak around 550–600 nm). Other than VivoTag 680, Liyi et al. [18] have shown that Cyanine 5.5-conjugated nanobubbles can be utilized as a dual ultrasound-fluorescence imaging contrast agent in a mouse model.

In the present study, we employed NIR fluorescent (VivoTag 680) labeling to investigate dynamic PVA-MB biodistribution using *in vivo* fluorescence imaging, and fluorescence microscopy for validation of distribution. The potential application of PVA-MBs as a contrast agent was also studied using ultrasound imaging in subcutaneous and orthotopic pancreatic cancer mouse models, to visualize blood flow inside living tumor masses.

2. Materials and methods

2.1. Synthesis of VivoTag 680 microbubbles

The PVA-MBs were manufactured as described previously [8,19,20]. Briefly, polyvinyl alcohol (PVA) was added to de-ionized water and dissolved followed by activation by sodium periodate. The solution was mixed with air using an Ultra Turrax T-25 (IKA-works, Inc., IKA-2000, Staufen, Germany) at 8000 rpm for 2 h in order to produce MBs. The MBs were washed 5 times using MilliQ water. The washing solution was removed through slow centrifugation (60 g, 30 min) then modified with aminoguanidine (AG) to enable further coupling. For that, 100 mL of the MB suspension (approximately 7.1×10^{10} MBs) were washed in 0.1 M HEPES buffer at pH = 8 (200 mL). Aminoguanidine (5 mg/mL) was added and the suspension was put on a shaker for three days followed by washing using the centrifuge. Thereafter, the aminoguanidine MBs (AG-MBs 12×10^9 MBs/ml) were washed and the supernatant removed. The MBs were made fluorescent by consecutive coating of a double layer of a sodium polystyrene sulfonate solution (PSS) and polyallylamine hydrochloride (PAH) by means of the layer-by-layer (LbL) technology under standard coating conditions (2 g/L polymer in 50 mM acetate buffer and 0.2 M NaCl, in a quantity of 3 mL/10^9 MB) to enable optical imaging. $NaHCO_3$ (5 mL, 50 mM) and VivoTag 680 (5 mg, Perkin–Elmer, Waltham, MA, USA) were added to the MBs to couple the dye to the outermost PAH layer. The suspension was stirred overnight and washed three times in the centrifuge followed by coating with one layer of negatively charged PSS, followed by three additional washing steps. The final concentration of the obtained VivoTag 680 MBs was 6.97×10^8 MBs/mL, adjusted to the standard value of 10^9 MBs/mL.

2.2. Cells

KPC cells were derived from the KrasLSL-G12D/+; p53R172H/+; Pdx1-Cre mouse model for human pancreatic ductal adenocarcinoma [21]. Cells were cultured in Dulbecco's modified Eagle's medium (DMEM)/F12 (1:1 mixture) (Gibco Life Technologies Europe BV), supplemented with 10% fetal bovine serum (Gibco Life Technologies Europe BV), 100 U/ml penicillin, 100 mg/ml streptomycin (Gibco Life Technologies Europe BV), at 37 °C and 5% CO_2.

2.3. Experimental animals

Female FVB/N mice (25 ± 2 g) were purchased from Charles River (Charles River Laboratories, Sulzfeld, Germany) and kept for one week in the animal facility to acclimatize before the experiments. They had access to food and water *ad libitum*, 12 h light/dark cycle, controlled humidity (55% ± 5%) and temperature (21 °C ± 2 °C).

Subcutaneous pancreatic tumor xenograft and orthotopic pancreatic tumor xenograft were established as previously described [13]. C57Bl/6J mice were obtained from Scanbur, Sweden, and used for all experiments at 6–8 weeks of age. Briefly, subcutaneous pancreatic tumor xenograft was established by *s.c.* injection of 2.5×10^5 KPC cells in a total volume of 50 μl phosphate buffered saline. Orthotopic pancreatic tumor xenograft was established by injection of 1×10^6 KPC cells (in 50 μl PBS) into the pancreatic tail using a 26 gauge needle. Mice were anesthetized via intra-peritoneal Ketamine (80 mg/kg) and Xylazine (8 mg/kg) injection and placed on a heating pad (40 °C) during surgery. Mice received pain relief with buprenorphine (0.06 mg/kg) for three consecutive days and 500 μl saline to restore the fluid balance. Two weeks after *s.c.* tumor inoculation/five weeks after orthotopic pancreatic tumor inoculation, mice were scanned as described below.

Prior to image acquisition, the mice were anaesthetized using 2–3% isoflurane (Baxter Medical AB, Kista, Sweden) and 1–2% isoflurane was used for anesthesia maintenance.

2.4. In vivo fluorescence imaging/computed tomography (CT)

The study was approved by the Stockholm Southern Ethical Committee on Animal Research (S89/12, S69/12 and S38/13 plus extensions) and performed in accordance with Swedish Animal Welfare law.

An IVIS® Spectrum (PerkinElmer, Waltham, MA, USA) was used for optical imaging and a Quantum FX for μCT imaging co-registration (PerkinElmer, Waltham, MA, USA). VivoTag 680 MBs (0.2 mL) were diluted (1:8) with NaCl (0.9%) and from that suspension 100 μl was intravenously injected into the lateral tail vein of mice (n = 12), corresponding to 0.5×10^6 MBs/mouse. The anesthetized mice were placed dorsal side up in a Mouse Imaging Shuttle (MIS; 25 mm high; PerkinElmer, Waltham, MA, USA) and imaged using IVIS 2D/3D-fluorescence imaging and Quantum FX-μCT at 30 min, 4 h and 24 h post injection. The MIS was used to transfer the mice from IVIS Spectrum to Quantum FX-μCT while maintaining their positions. Mice were first imaged with a fast 2D-fluorescent imaging protocol and analysis by spectral un-mixing to separate tissue auto-fluorescence from light emitted from the VivoTag 680 dye.

Thereafter, the mice were imaged in the MIS using 3D-Fluorescent Imaging Tomography (FLIT) with trans-illumination. The 3D-

FLIT imaging sequence was set up and acquired at excitation 675 nm and emission 720 nm. The mouse in the MIS was then transferred to the Quantum FX-μCT and subjected to a fast, low dose CT-scan with a field of view (FOV) at 75 mm and 17-s scan time. After the imaging sessions, three mice were sacrificed and their removed organs (lungs, liver, spleen and kidneys) were imaged *ex vivo* using 2D-fluorescent imaging employing a filter pair of 675/720 nm and fluorescence efficiency quantification. All images were generated using Living Image® 4.4 software (PerkinElmer, Waltham, MA, USA).

2.5. Ultrasound imaging

All ultrasound (US) scanning was performed on a VisualSonics Vevo LAZR Imaging Station (VisualSonics, Inc., Toronto, Canada) as previously described [13]. Mice were anesthetized using 1.5% isoflurane with medical air at a flow of 2 L/min. Hair was removed over areas of interest using a depilatory cream. US gel (Parker Laboratories Inc., Fairfield, NJ, USA) was applied over the region of interest. ECG, respiration, blood pressure, and body temperature were monitored during image acquisition. Nonlinear contrast imaging was acquired using the LZ250 transducer at a frequency of 18 MHz, power of 4%, immediately after an intravenous bolus injection of 100 μl MBs at a concentration of 1×10^9/ml (1×10^8 MBs/mouse). A cine loop was recorded at a frame rate of 17/sec for liver and orthotopic tumor, 22/sec for *s.c.* tumor.

2.6. Necropsy and histology

Histologic analysis of livers, kidneys, spleens and lungs was performed using bright field and fluorescence microscopy. To verify observations from the different live imaging modalities, the organs were removed, fixed in paraformaldehyde (4%) for 48 h, then transferred to ethanol (70%), routinely processed and embedded in paraffin. Thereafter, tissue sections (4 μm) were mounted on superfrost glass slides. Slides were routinely stained with hematoxylin & eosin (HE) for bright field microscopy, or left unstained and mounted with 4′,6-diamidino-2-phenylindole (DAPI) containing mounting medium (Vector VECTASHIELD H1200) to produce nuclear counter stain for fluorescence microscopic evaluation.

3. Results

3.1. In vivo fluorescence imaging/computed tomography (CT)

The NIR property of VivoTag 680 makes the fluorescently labeled microbubbles (VivoTag 680 MBs) suitable for *in vivo* fluorescence imaging. Fig. 1 shows the morphology and fluorescent signal of VivoTag 680 MBs as observed by confocal microscopy. In order to assess the biodistribution of microbubbles, VivoTag 680 MBs were intravenously injected into mice. Their distribution was monitored over 24 h using an IVIS Spectrum and the 3D-Fluorescent Imaging Tomography (FLIT) was co-registered with 3D-μCT images for anatomical referencing (Fig. 2A). Images were acquired at 30 min, 4 h and 24 h post injection. With the combination of fluorescence imaging and μCT imaging, the uptake and biodistribution of VivoTag 680 MBs in different organs was detected in living animals over time with high sensitivity. Initially (30 min) the MBs accumulated primarily in the lungs, as this is the first capillary network they encounter after tail vein injection. At 4 h post injection, the fluorescence signal was still mainly seen in the lungs and to some minor extent in the liver. At 24 h, a strong signal was observed in both lungs and liver, followed by spleen and kidneys. The *ex vivo* examination of the organs (Fig. 2B) showed decreased fluorescent intensity in the lungs by time and the redistribution to the liver, spleen and kidneys.

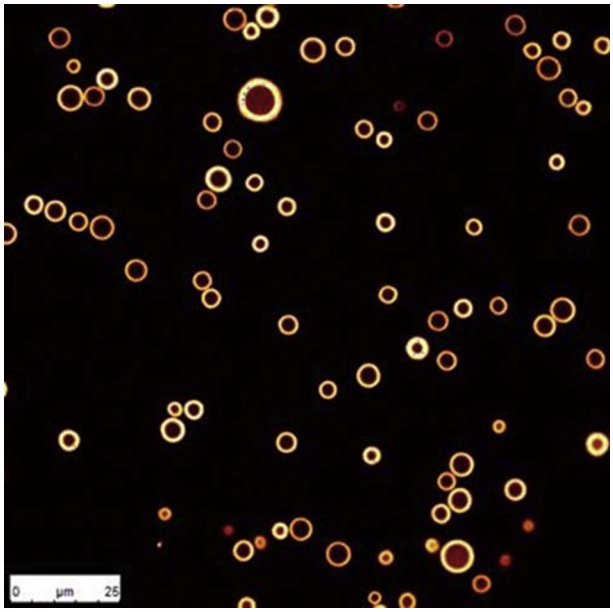

Fig. 1. VivoTag 680 MBs imaged after production using confocal microscopy. Image size 138 × 138 μm, Leica TCS SPE confocal laser scanning microscope, Leica microsystems GmbH, Germany.

3.2. Ultrasound

Next, we tested if the PVA-MBs are functional in live contrast imaging of small animals. Nonlinear contrast imaging mode was chosen for MB detection since it better differentiates the acoustic signal from MBs from surrounding tissue at low ultrasound power without disrupting the MBs. Fig. 3A shows the contrast enhancement in mouse liver after bolus *i.v.* MB injection at a dosage of 1×10^8 MBs/mouse. Region of interest (ROI) is drawn over the liver and MB wash-in curve over the ROI is illustrated as contract mean power (a.u.) vs. time (sec) after bolus injection. A clear contrast signal increase in the liver was observed with a peak enhancement of 10% compared to the baseline. Pancreatic ductal adenocarcinoma (PDAC) is known to be highly stromal-enriched and poorly vascularized, which leads to inefficient drug delivery at the tumor site and treatment failure in most patients [22]. Mouse PDAC xenograft models were engaged to test the potential application of PVA-MBs in real time tumor perfusion measurement. Syngeneic PDAC mouse models were established by injection of KPC cells into C57Bl/6J mice subcutaneously/orthotopically. Fig. 3B (S-Video 1) shows the overlay of contrast mode imaging (Green scale) to B-mode imaging (Gray scale) in *s.c.* KPC tumor, 30 s after bolus *i.v.* injection of PVA-MBs at a dosage of 1×10^8 MBs/mouse. Blood flow is only observed in the surrounding area of the *s.c.* tumor but not inside the tumor mass. Fig. 3C (S-Video 2) shows blood perfusion in an orthotopic KPC tumor. Similar to the *s.c.* tumor, MB filtration is only visualized in the surrounding normal pancreas tissue and kidney, but not inside the tumor mass. PVA-MBs successfully demonstrated the poorly vascularized feature of PDAC, in both subcutaneous and orthotopic KPC xenograft models.

Supplementary video related to this article can be found at http://dx.doi.org/10.1016/j.bbrc.2015.07.017.

3.3. Histology

Microscopic analysis confirmed the presence of scattered, variably sized groups of microbubbles in the lungs, liver, spleen and kidney (Fig. 4, fluorescence microscopy with bright field

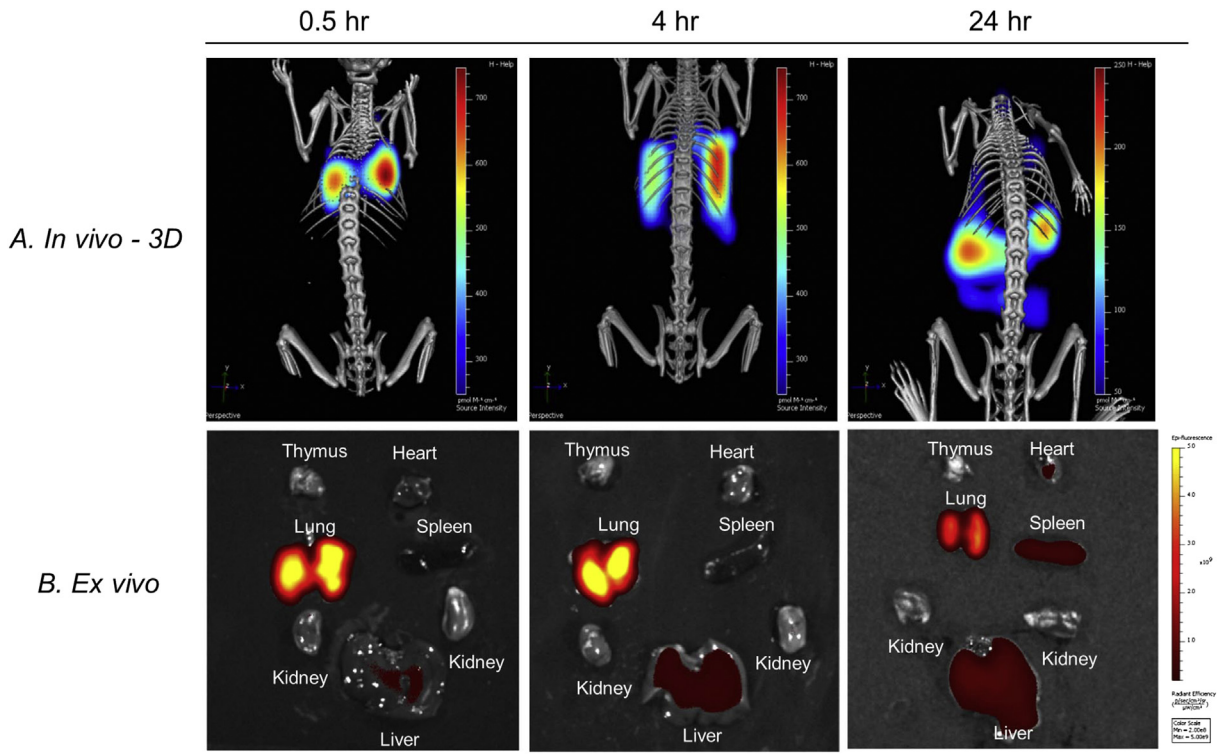

Fig. 2. 3D *in vivo* and *ex vivo* fluorescence imaging at 30 min-24 h post injection. Fluorescence imaging using IVIS® Spectrum (PerkinElmer) post injection of VivoTag 680 MBs. A. Co-registration of 3D fluorescence images with μCT images (Quantum FX, PerkinElmer) at 0.5 h, 4 h and 24 h post injection. B. Corresponding *ex vivo* organ fluorescence images at 0.5 h, 4 h and 24 h post injection.

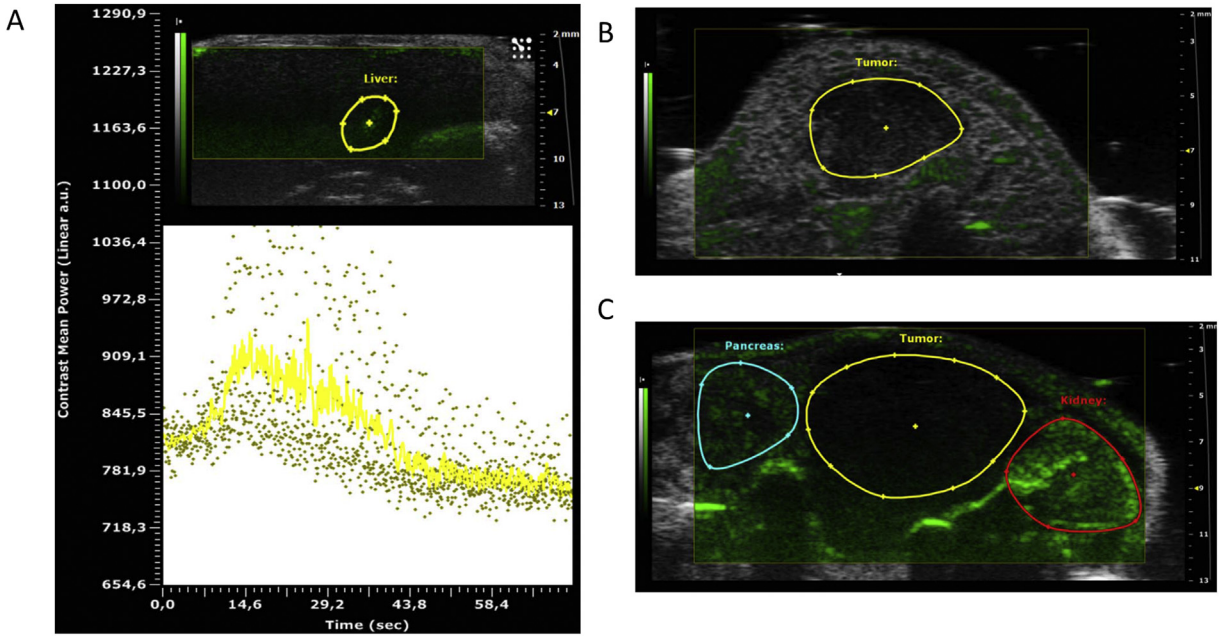

Fig. 3. Nonlinear contrast imaging with PVA-MBs as contrast agent in ultrasound. B-mode images (Gray scale) are overlaid simultaneously with nonlinear contrast images (Green scale). **A**. Nonlinear contrast image and PVA-MB wash-in curve in mouse liver after PVA-MB intravenous injection. **B**. Nonlinear contrast image in *s.c.* KPC tumor at 30sec after PVA-MB intravenous injection. Region of interest: Yellow, tumor. C. Nonlinear contrast image in orthotopic pancreatic KPC tumor at 30 s after PVA-MB intravenous injection. Regions of interest: Yellow, tumor; Green, pancreas; Red, kidney. (For interpretation of the references to colour in this figure legend, the reader is referred to the web version of this article.)

background showing tissue structure in addition to red signal for VivoTag 680 MBs and blue for DAPI nuclear counter stain). Routine HE staining (data not shown) revealed that in the lungs, bubbles were present from the first investigated time point as single bubbles in septal capillaries and as small endocytosed clusters in alveolar/interstitial macrophages. Notably, from 2 h following injection, larger clusters of microbubbles appeared in larger arterioles associated with fibrillary, eosinophilic intravascular occlusive

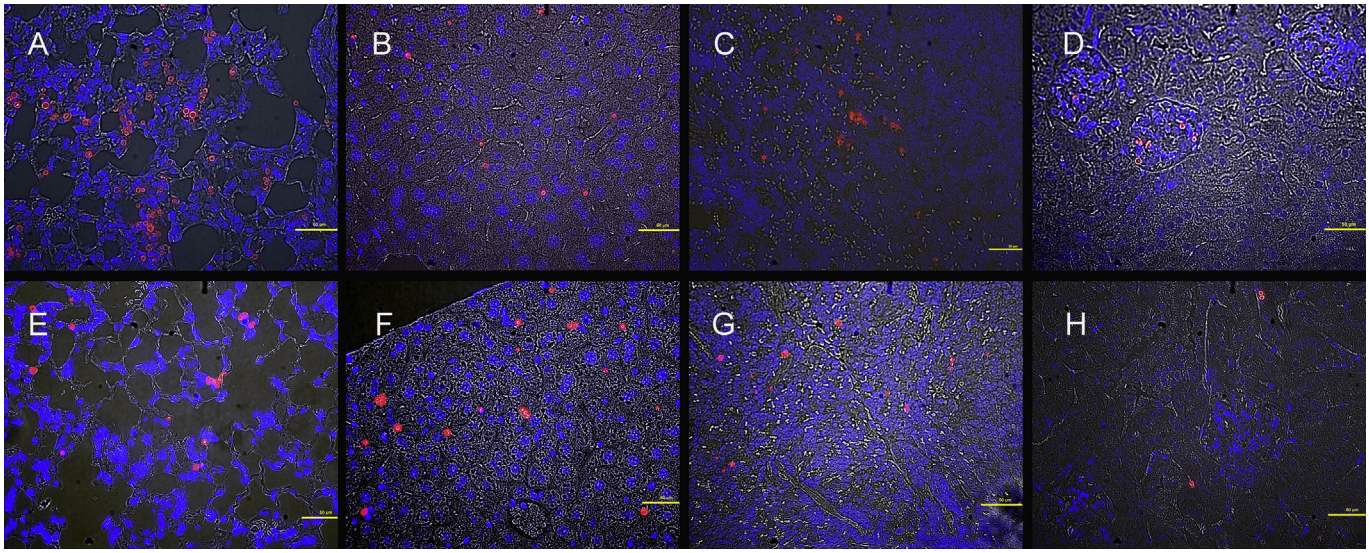

Fig. 4. Fluorescence microscopy overlaid bright field images of organs. Fluorescence images of VivoTag 680 MBs are shown in red while nuclei are stained with (DAPI) using 4′,6-diamidino-2-phenylindole. Organs: Lung (A, 30 min; E, 24 h); liver (B, 30 min; F, 24 h); spleen (C, 30 min; G, 24 h) and kidney (D, 30 min; H, 24 h). Scale bar, 50 μm. (For interpretation of the references to colour in this figure legend, the reader is referred to the web version of this article.)

material, consistent with fibrin thrombo-emboli. All mice showed increased cellularity in the pulmonary septa with predominantly macrophage accumulation, from 2 h onwards more clearly accompanied by neutrophils and some lymphocytes. One mouse at 2-, one at 4- and two mice at 24 h showed multifocal pulmonary hemorrhage.

In the liver, groups of generally 2–4 MBs were observed associated with sinusoidal Kupffer cells from the first investigated time point on. There was no marked increase in density of hepatic MBs over time as indicated by classical histology and fluorescence microscopy in microscopically investigated organs. In the spleen, MBs were also found mainly in association with tentative macrophages, most commonly in the marginal zone.

Kidneys at 30 min after MB injection show glomerular hyperemia, occasional glomerular hemorrhage and occasional glomerular and rare interstitial MBs. After 4 h following injection, glomeruli showed degenerative changes with occasional protein loss in Bowman's capsule. From 4 h after injection on, occasional degenerated and sometimes small, fragmented (atrophic) glomeruli were observed. There was frequent vacuolar degeneration of outer medullary tubule segments and moderate luminal protein casts at every time point.

4. Discussion

We successfully labeled PVA-MBs with the near infrared (NIR) fluorophore VivoTag 680 to enable fluorescence imaging of MBs in small animals using 3D-fluorescence imaging tomography (IVIS). For anatomic structure reference points, μCT was utilized for co-registration. Tomographic 3D-fluorescence imaging facilitates the detection of fluorescence labeled compounds with good sensitivity. However, as is the case in nuclear medicine imaging, the anatomical information is missing. CT has inherent spatial resolution and excellent signal-to-noise performance, and can therefore provide anatomical reference points. Previous studies in rats demonstrated that additional incorporation of SPION renders PVA microbubbles detectable by MRI, providing a radiation-free alternative anatomic reference for accurate signal localization [23]. In the current study, we demonstrate that fluorescence/μCT imaging can show the presence/accumulation of fluorescent MBs over time in lungs, liver and kidneys in mice. As previously shown in fluorescently labeled bacteria and injected cells, longer wavelength near infra-red fluorescence is particularly suited for imaging of deeper anatomical structures. Since the fluorescent signal from VivoTag 680 MBs enabled detection in the liver and even in the lungs (where alveolar air content prevents visualization by ultrasound), near infra-red fluorescence adds an imaging modality that could be essential for preclinical evaluation of future targeting of hepatic and pulmonary tumor metastases. After 24 h, the VivoTag 680 fluorescence was no longer visible in the lungs using 3D-fluorescence imaging, but had redistributed to the liver and spleen of the mice. However, the *ex vivo* scan using 2D-fluorescence imaging still showed a high amount of fluorescence in the lungs compared to the liver. This could be a result of hemostasis in the lungs as well as local hyperemia and congestion [24].

MB targeting efficiency and off-target accumulation is significantly affected by biodistribution characteristics. Nuclear imaging techniques such as positron emission tomography (PET) and SPECT are useful tools to examine the biodistribution of radio-labeled imaging agents with high spatial resolution. In our previous studies, biodistribution, kinetics and biological fate of MBs were evaluated with a combination of multiple nuclear imaging modalities, SPECT/CT and MRI. Compared to SPECT or PET, optical imaging is less complicated, safer for the operator and has a lower threshold for achieving high throughput for pre-clinical studies. Unlike nuclear imaging, fluorescence imaging does not involve radio-labeling; therefore, no hot lab is required and there is no risk of radiation exposure of personnel. However, due to light scattering and light absorption by tissue, optical imaging is still limited to small animals.

One of the main MB applications in preclinical ultrasound imaging is as a contrast agent to visualize blood flow in living animals, especially for tumor angiogenesis studies. After intravenous administration into the blood circulation, gas-filled MBs can be favorably detected by ultrasound over the surrounding tissue. Pancreatic ductal adenocarcinoma (PDAC) is known to be highly stromal-enriched and poorly vascularized. A mouse PDAC/KPC model has been proved by contrast imaging with commercial MBs, such as Vevo MicroMarker contrast agent, to have angiogenesis properties similar to human PDAC [22]. This study uses mouse PDAC/KPC xenograft models to test the potential application of PVA-MBs in real time tumor perfusion measurement. Our results

show that air-filled PVA-MBs can also successfully overcome the poor vascularization of PDAC in both subcutaneous and orthotopic KPC xenograft models.

Similar to other studies including a modified version of PVA-MBs [6,8,25,26], the present study shows high potential for MBs in multimodal imaging. An advantage of having a contrast/reporter agent that can be visualized with several modalities is the increased diagnostic value when anatomic, functional and target specific imaging can be provided.

In our investigation, we showed that PVA-MBs can be labeled with VivoTag 680 and utilized for multimodal imaging using optical imaging as well as ultrasound in mice. In vivo fluorescence images co-registered with CT-images localized the fluorescent signal from internal and air-containing organs. VivoTag 680 MBs were found to be distributed mainly to the lungs within the first 4 h then re-distributed to the liver, spleen and kidneys within 24 h. The microbubbles are indeed an important contrast agent; however, studies for the optimization of the size and echogenicity of the MBs are warranted to minimize their time in the lungs and to evaluate their potency as drug carriers.

In summary, PVA-MBs originally developed as an ultrasound contrast agent can be labelled with near infra-red fluorescence and used as a contrast agent in deeper and air containing tissues. The development of multimodal contrast agents opens the possibility of studying targeted treatment and of following up therapeutic efficacy in preclinical studies. Potential use of the MBs as theranostics should be considered; however, hemodynamic hemostatic effects of the MBs following intravenous injection need to be addressed.

Conflict of interest

None.

Acknowledgments

The authors express their gratitude to: The Swedish Childhood Cancer Society (BCF) (PROJ11/112) and The Swedish Cancer Foundation (CF) (09 0412 and 12 0441).

Transparency document

Transparency document related to this article can be found online at http://dx.doi.org/10.1016/j.bbrc.2015.07.017.

References

[1] S. Unnikrishnan, A.L. Klibanov, Microbubbles as ultrasound contrast agents for molecular imaging: preparation and application, AJR Am. J. Roentgenol. 199 (2012) 292–299.
[2] P. Ghosh, G. Han, M. De, C.K. Kim, V.M. Rotello, Gold nanoparticles in delivery applications, Adv. Drug Deliv. Rev. 60 (2008) 1307–1315.
[3] M.J. Hawkins, P. Soon-Shiong, N. Desai, Protein nanoparticles as drug carriers in clinical medicine, Adv. Drug Deliv. Rev. 60 (2008) 876–885.
[4] Y. Liu, H. Miyoshi, M. Nakamura, Novel drug delivery system of hollow mesoporous silica nanocapsules with thin shells: preparation and fluorescein isothiocyanate (FITC) release kinetics, Colloids Surf. B Biointerfaces 58 (2007) 180–187.
[5] Y. Liu, H. Miyoshi, M. Nakamura, Nanomedicine for drug delivery and imaging: a promising avenue for cancer therapy and diagnosis using targeted functional nanoparticles, Int. J. Cancer 120 (2007) 2527–2537.
[6] A.A. Barrefelt, T.B. Brismar, G. Egri, P. Aspelin, A. Olsson, L. Oddo, S. Margheritelli, K. Caidahl, G. Paradossi, L. Dahne, R. Axelsson, M. Hassan, Multimodality imaging using SPECT/CT and MRI and ligand functionalized 99mTc-labeled magnetic microbubbles, EJNMMI Res. 3 (2013) 12.
[7] Å. Barrefelt, G. Paradossi, H. Asem, S. Margheritelli, M. Saghafian, L. Oddo, M. Muhammed, P. Aspelin, M. Hassan, T.B. Brismar, Dynamic MR imaging, biodistribution and pharmacokinetics of polymer shelled microbubbles containing SPION, Nano 0 (2014) 1450069.
[8] A. Barrefelt, M. Saghafian, R. Kuiper, F. Ye, G. Egri, M. Klickermann, T.B. Brismar, P. Aspelin, M. Muhammed, L. Dahne, M. Hassan, Biodistribution, kinetics, and biological fate of SPION microbubbles in the rat, Int. J. Nanomed. 8 (2013) 3241–3254.
[9] D. Grishenkov, L. Kari, L.K. Brodin, T.B. Brismar, G. Paradossi, In vitro contrast-enhanced ultrasound measurements of capillary microcirculation: comparison between polymer- and phospholipid-shelled microbubbles, Ultrasonics 51 (2011) 40–48.
[10] D. Grishenkov, C. Pecorari, T.B. Brismar, G. Paradossi, Characterization of acoustic properties of PVA-shelled ultrasound contrast agents: ultrasound-induced fracture (part II), Ultrasound Med. Biol. 35 (2009) 1139–1147.
[11] D. Grishenkov, C. Pecorari, T.B. Brismar, G. Paradossi, Characterization of acoustic properties of PVA-shelled ultrasound contrast agents: linear properties (part I), Ultrasound Med. Biol. 35 (2009) 1127–1138.
[12] M. Larsson, M. Larsson, L. Oddo, S. Margheritelli, G. Paradossi, J. Nowak, L.A. Brodin, K. Caidahl, A. Bjallmark, Visualization of multimodal polymer-shelled contrast agents using ultrasound contrast sequences: an experimental study in a tissue mimicking flow phantom, Cardiovasc. Ultrasound 11 (2013) 33.
[13] M. Gerling, Y. Zhao, S. Nania, K.J. Norberg, C.S. Verbeke, B. Englert, R.V. Kuiper, A. Bergstrom, M. Hassan, A. Neesse, J.M. Lohr, R.L. Heuchel, Real-time assessment of tissue hypoxia in vivo with combined photoacoustics and high-frequency ultrasound, Theranostics 4 (2014) 604–613.
[14] Z.R. Luo, T. Huang, W. Li, B.Z. Shen, Use of in vivo imaging system-bioluminescence imaging to inspect tumor dynamic morphology, Panminerva Medica 52 (2010) 1–7.
[15] K.O. Vasquez, C. Casavant, J.D. Peterson, Quantitative whole body biodistribution of fluorescent-labeled agents by non-invasive tomographic imaging, Plos One 6 (2011).
[16] P. Koczera, Z. Wu, S. Fokong, B. Theek, L. Appold, S. Jorge, D. Mockel, Z. Liu, A. Curaj, G. Storm, M. van Zandvoort, F. Kiessling, T. Lammers, Fluorescently labeled microbubbles for facilitating translational molecular ultrasound studies, Drug Deliv. Transl. Res. 2 (2012) 56–64.
[17] M. Liang, X. Liu, D. Cheng, G. Liu, S. Dou, Y. Wang, M. Rusckowski, D.J. Hnatowich, Multimodality nuclear and fluorescence tumor imaging in mice using a streptavidin nanoparticle, Bioconjug. Chem. 21 (2010) 1385–1388.
[18] L. Mai, A. Yao, J. Li, Q. Wei, M. Yuchi, X. He, M. Ding, Q. Zhou, Cyanine 5.5 conjugated nanobubbles as a tumor selective contrast agent for dual ultrasound-fluorescence imaging in a mouse model, PLoS One 8 (2013) e61224.
[19] C.S. Peyratout, L. Dahne, Tailor-made polyelectrolyte microcapsules: from multilayers to smart containers, Angew. Chem. Int. Ed. Engl. 43 (2004) 3762–3783.
[20] F. Cavalieri, A. El Hamassi, E. Chiessi, G. Paradossi, Stable polymeric microballoons as multifunctional device for biomedical uses: synthesis and characterization, Langmuir 21 (2005) 8758–8764.
[21] A. Neesse, K.K. Frese, T.E. Bapiro, T. Nakagawa, M.D. Sternlicht, T.W. Seeley, C. Pilarsky, D.I. Jodrell, S.M. Spong, D.A. Tuveson, CTGF antagonism with mAb FG-3019 enhances chemotherapy response without increasing drug delivery in murine ductal pancreas cancer, Proc. Natl. Acad. Sci. U. S. A. 110 (2013) 12325–12330.
[22] E. Huynh, C.S. Jin, B.C. Wilson, G. Zheng, Aggregate enhanced trimodal porphyrin shell microbubbles for ultrasound, photoacoustic, and fluorescence imaging, Bioconjug. Chem. 25 (2014) 796–801.
[23] A. Zelmer, P. Carroll, N. Andreu, K. Hagens, J. Mahlo, N. Redinger, B.D. Robertson, S. Wiles, T.H. Ward, T. Parish, J. Ripoll, G.J. Bancroft, U.E. Schaible, A new in vivo model to test anti-tuberculosis drugs using fluorescence imaging, J. Antimicrob. Chemother. 67 (2012) 1948–1960.
[24] B.W. Rice, M.D. Cable, M.B. Nelson, In vivo imaging of light-emitting probes, J. Biomed. Opt. 6 (2001) 432–440.
[25] J. Härmark, M.K. Larsson, A. Razuvajev, P.J.B. Koeck, G. Paradossi, L.-Å. Brodin, et al., Investigation of the elimination process of a multimodal polymer-shelled contrast agent in rats using ultrasound and transmission electron microscopy, Biomed. Spectrosc. Imaging 4 (2015) 81–93.
[26] T.B. Brismar, D. Grishenkov, B. Gustafsson, J. Harmark, A. Barrefelt, S.V. Kothapalli, S. Margheritelli, L. Oddo, K. Caidahl, H. Hebert, G. Paradossi, Magnetite nanoparticles can be coupled to microbubbles to support multimodal imaging, Biomacromolecules 13 (2012) 1390–1399.